Received: 19 June 2019 | Revised: 27 November 2019 | Accepted: 6 December 2019

DOI: 10.1111/ter.12447

PAPER

Terra Nova WILEY

Formation and metamorphism of sedimentary rocks beneath the Dingxi Basin: Record of the evolution from subduction to collision in the North Qilian Orogen

Bin Wang[1,2] | Wei-(RZ) Wang[2] | Zuoling Tian[3] | Chunjing Wei[1] | Yue Zhao[2]

[1]MOE Key Laboratory of Orogenic Belts and Crustal Evolution, School of Earth and Space Sciences, Peking University, Beijing, China

[2]Key Laboratory of Paleomagnetism and Tectonic Reconstruction of MONR, Institute of Geomechanics, Chinese Academy of Geological Sciences, Beijing, China

[3]Institute of Geology, Chinese Academy of Geological Sciences, Beijing, China

Correspondence
Wei-(RZ) Wang, Institute of Geomechanics, Chinese Academy of Geological Sciences, Beijing 100081, China.
Email: Wangwei0521@gmail.com

Funding information
National Natural Science Foundation of China, Grant/Award Number: 41202047 and 41672062; Fundamental Research Funds of CAGS, Grant/Award Number: JYYWF201819

Abstract

The North Qilian Orogen (NQO) in northwest China underwent oceanic subduction and subsequent continental collision. Metasedimentary rocks from a deep borehole in the Dingxi Basin, NQO, contain garnet, biotite, plagioclase, quartz and minor cummingtonite and chlorite in the matrix, with inclusions of kyanite and staurolite in garnet. The mineral textures and compositions define clockwise pressure–temperature evolution with peak conditions of ~10.5 kbar and ~670°C, followed by isothermal decompression down to ~6.5 kbar. Age and Hf isotope data of detrital zircon support the formation of the sedimentary protolith in an arc setting at ~460 Ma, and the age and rare earth element characteristics of metamorphic monazite reflect exhumation at ~425 Ma. These results indicate a complete cycle of deposition–burial–exhumation for the sedimentary rocks, and directly constrain the continental collision process in NQO to yield a geotherm of ~21°C/km and to culminate before 425 Ma.

1 | INTRODUCTION

The Earth's crust can be altered by deformation, metamorphism and magmatism during orogenesis (Brown, 2001). Metamorphic rocks exposed at the Earth's surface and concealed by sedimentary cover are very crucial to a thorough understanding of the thermo–depth–time evolution of ancient orogens. As a classic case, metamorphic rocks in the North Qilian Orogen (NQO) record various stages from spreading, through subduction, to closure of the North Qilian Ocean, and the subsequent continental collision between the Qilian–Qaidam block and the Alashan block during the early Palaeozoic (e.g. Chen, Song, Niu, & Wei, 2014; Song, Niu, Su, & Xia, 2013; Yang, Du, Cawood, & Xu, 2012). The low temperature–high pressure (LT–HP) metamorphic rocks (e.g. eclogites and blueschists) well reflect and constrain the earlier oceanic subduction (Song et al., 2007; Wei & Song, 2008; Wei, Yang, Su, & Song, 2009; Zhang, Meng, & Wan, 2007); however, the later continental collision has not been directly constrained except by inference from the Devonian molasse (e.g. Song et al., 2013). The lack of exposed metamorphic rocks recording the collision stage in the orogen hinders understanding of the key processes of the orogenesis. In this study, metasedimentary rocks were sampled from a deep borehole under the Dingxi Basin at the eastern end of NQO, and investigated by integrated petrologic, thermodynamic, chronologic and isotopic analyses/calculations. The findings help to define the nature of the metasedimentary rocks beneath the Dingxi Basin and provide critical constraints on the evolution of NQO.

2 | GEOLOGIC SETTING AND SAMPLING

The North Qilian Orogen is located in northwest China, which extends NW–SE for ~ 1,200 km. Bordered by the Alashan Block to the north and the Qilian Block to the south, the orogen is offset by the Altyn Tagh Fault to the northwest and intersected by the North China Craton at its eastern end (Figure 1a). The main rocks in NQO include Neoproterozoic to early Palaeozoic ophiolite sequences, LT–HP metamorphic rocks, arc volcanic rocks and granitoid plutons, Silurian flysch formations, Devonian molasse and Carboniferous to Triassic sedimentary cover sequences (Wu, Feng, Huo, & Zuo, 1990; Wu, Feng, & Song, 1993; Feng &

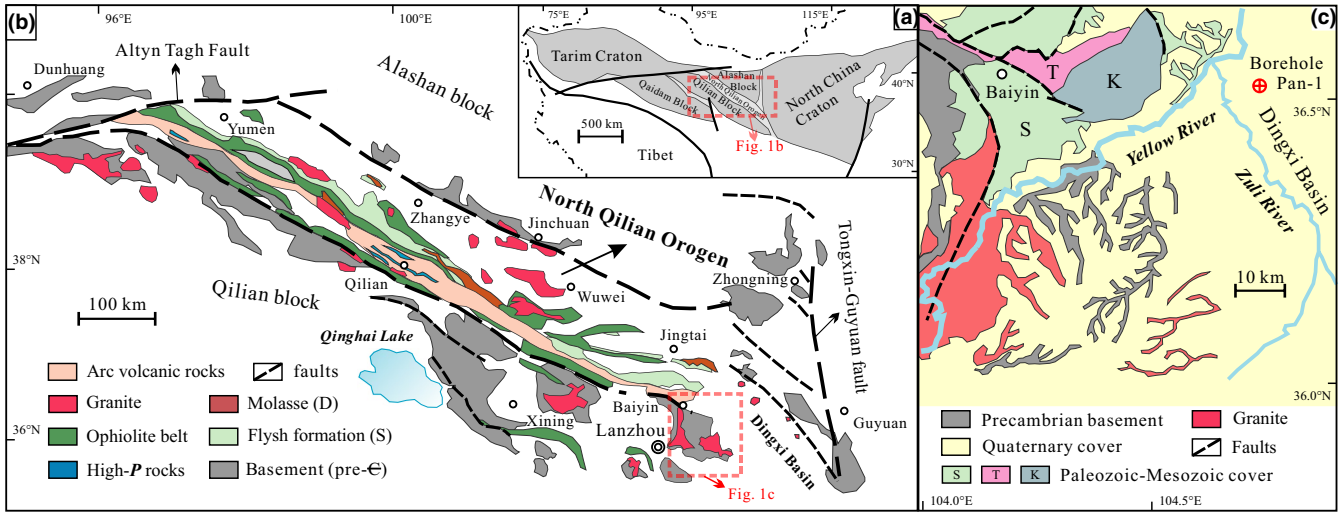

FIGURE 1 (a) Tectonic location of the North Qilian Orogen (modified after Song et al., 2013). (b) Lithologic distribution within the North Qilian Orogen (modified after Song et al., 2013; Yang et al., 2015). (c) Locality of the Pan-1 borehole (modified after Wu et al., 2018). (Abbreviations: pre-Є, Precambrian; S, Silurian; D, Devonian; T, Triassic; K, Cretaceous) [Colour figure can be viewed at wileyonlinelibrary.com]

He, 1996; Song, 1996; Zhang, Xu, Chen, & Xu, 1997; Zhang, Sun, et al., 1997; Zhang, Chen, & Zhou, 1998; Figure 1b). The ophiolite sequences have different crystallization ages of 550 ± 17 Ma (Shi, Yang, & Wu, 2004), 504–490 Ma (Tseng et al., 2007; Xia & Song, 2010; Xiang et al., 2007) and 449 ± 5 Ma (Song et al., 2013). The well-preserved ophiolite sequences have been interpreted to represent the remnants of ancient oceanic lithosphere; thus NQO is generally accepted as an early Palaeozoic typical oceanic suture zone. The LT–HP metamorphic rocks mainly occur as eclogites and blueschists, which have major HP metamorphic ages of 489–463 Ma (Song et al., 2004; Zhang et al., 2007) and 466–454 Ma (Liou, Wang, Coleman, Zhang, & Maruyama, 1989; Zhang, Xu, et al., 1997) respectively, and were exhumed at 400–420 Ma (Lin, Zhang, Ji, & Song, 2010; Liu et al., 2006). The LT–HP metamorphism in NQO recorded an early "cold" oceanic subduction with a geotherm of ~7°C/km (Song et al., 2007; Wei & Song, 2008; Wei et al., 2009; Zhang et al., 2007). The Devonian molasse, which consists of terrestrial conglomerates and sandstones unconformably, overlies the earlier rock series and was interpreted to have deposited in an intermountain or foreland basin in response to the continental collision between the Qilian–Qaidam block and the Alashan block (e.g. Song et al., 2013).

Located at the eastern end of NQO (Figure 1b), the Dingxi Basin is covered by sedimentary sequences formed in Silurian, Triassic, Cretaceous and Quaternary (Figure 1c; Wu, Deng, Kong, & Liu, 2018). The deep borehole Pan-1 in the Dingxi Basin penetrated into the underlying metamorphic rocks. Sample P1-4 was collected from a depth of 1115–1118 m (Figure S1a).

3 | PETROLOGIC ANALYSES

3.1 | Petrography and mineral composition

The basement samples are massive with weak foliation, and lack any textural evidence of partial melting (e.g. leucosome). Sample P1-4 consists mainly of garnet (g), biotite (bi), plagioclase (pl) and quartz (q), with minor kyanite (ky), staurolite (st), cummingtonite (cum), chlorite (chl) and Ti–Fe oxides (rutile, ru; ilmenite, ilm).

Garnet porphyroblasts are generally subhedral and ~2.5 mm across. They contain inclusions of biotite, staurolite, plagioclase, kyanite and rutile (Figure 2a; S1b,c). Garnet compositions are dominated by almandine (64–68 mol%) and pyrope (22–26 mol%) with relatively low spessartine (3.0–3.9 mol%) and grossular (5.9–7.0 mol%), with $Mg^{\#}$ [= 100 Mg/(Mg + Fe^{2+})] of 24.8–29.1 and X_{Ca} [= 100 Ca/(Ca + Mg + Fe^{2+})]

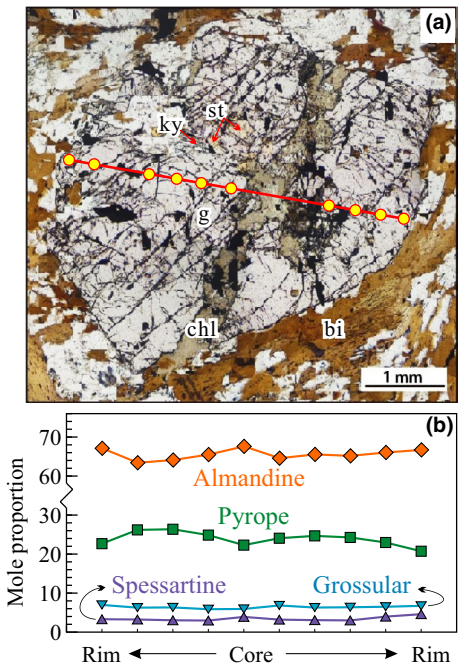

FIGURE 2 Minerals associated with garnet and the component profile of garnet. (Abbreviations: bi, biotite; chl, chlorite; g, garnet; ky, kyanite; st, staurolite) [Colour figure can be viewed at wileyonlinelibrary.com]

of 6.2–7.2 (Table S1). Garnet porphyroblasts exhibit compositional zoning (Figure 2), with decreasing almandine, grossular and spessartine and increasing pyrope from core to mantle and an opposite trend from mantle to rim (Figure 2b). The mantle-to-rim garnet compositional profile may represent diffused zoning during the post-peak retrograde stage (e.g. Spear, Kohn, Florence, & Menard, 1991).

Plagioclase occurs in the matrix or as inclusions in garnet (Figure S1c,d); the matrix crystals display lower An (anorthite) contents (31.3–33.9 mol%; Table S1) than the inclusions (~86.5 mol%). Biotite is present as flakes in the matrix and as inclusions in garnet (Figure 2a; S1b); both types exhibit similar compositions with $Mg^{\#}$ of 60–61 and Ti of 0.092–0.116 cations per formula unit (p.f.u.) (Table S1). Staurolite occurs as inclusions in garnet, wih $Mg^{\#}$ of 23–24. Cummingtonite occurs as fibrous aggregations in the matrix (Figure S1e), with $Mg^{\#}$ of 56–57.

Based on these mineral textures, the mineral paragenesis was inferred as follows. The pre-peak or peak assemblage is preserved as garnet inclusions and contains staurolite, kyanite and rutile. The retrograde assemblage, which occurs only in the matrix, contains cummingtonite, chlorite and ilmenite. Quartz, plagioclase, biotite and garnet may exist through all these assemblages.

3.2 | Bulk-rock composition

Sample P1-4 is characterized by enriched ferromagnesian contents (18.3–19.4 wt%, $Mg^{\#}$ = ~52) and low proportional levels of silica (49.78–52.24 wt%). It contains Al_2O_3 of 16.49–17.74 wt%, yielding A/CNK [Al_2O_3/(CaO + Na_2O + K_2O)] values of 1.33–1.38. For trace elements (Table S2), the chondrite-normalized rare earth elements (REE) show a pattern with tenfold to hundredfold enrichment of light REE and approximately tenfold enrichment of heavy REE (Figure S2). The PAAS (post-Archaean Australia shale)-normalized REE pattern shows a nearly flat shape (around 1) with slight positive Eu anomalies, suggesting a sedimentary origin of the protolith, which is further supported by detrital zircon analyses (see below).

4 | PHASE EQUILIBRIA MODELLING

The pressure–temperature (*P–T*) pseudosection was calculated for a *P–T* range of 5–13 kbar and 600–700°C (Figure 3). The water-saturated solidus occurs at ~ 680°C/10 kbar (Figure 3a). Quartz, plagioclase and

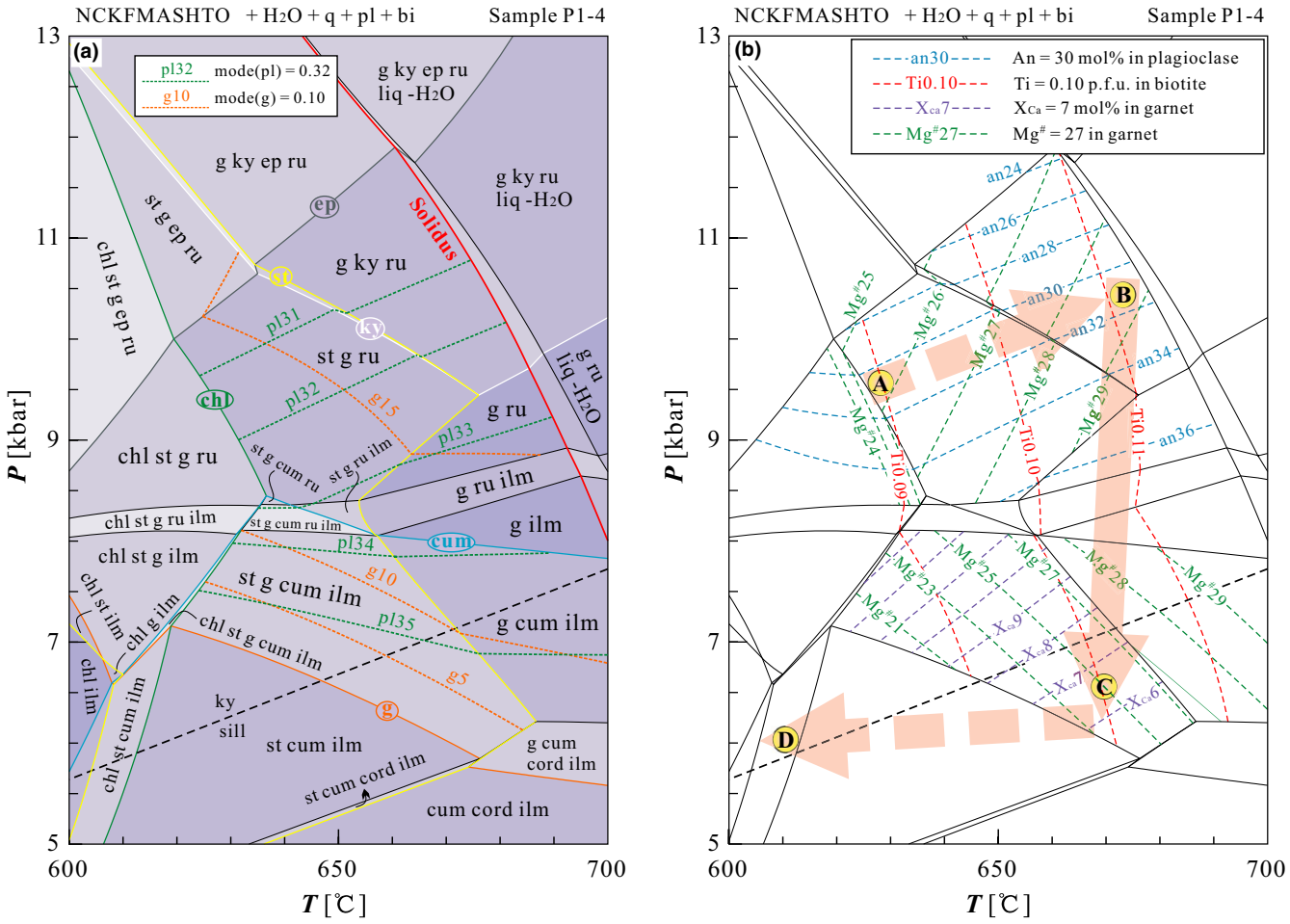

FIGURE 3 *P–T* pseudosection for sample P1-4. (a) Phase equilibria relations with mineral stability ranges and modes of garnet and plagioclase. (b) Compositional isopleths of relevant minerals with proposed *P–T* path. (Abbreviations: bi, biotite; chl, chlorite; cord, cordierite; cum, cummingtonite; ep, epidote; g, garnet; ilm, ilmenite; ky, kyanite; pl, plagioclase; ru, rutile; st, staurolite) [Colour figure can be viewed at wileyonlinelibrary.com]

biotite are stable over the whole *P–T* window and constitute the dominant minerals of the rock. Garnet is predicted to be absent at pressures below 5.5–7 kbar. The rutile–ilmenite transition occurs at a pressure of 8–9 kbar, kyanite is stable at pressures above ~9.5 kbar, and cummingtonite appears at pressures below ~ 8 kbar (Figure 3a). Chlorite is stable at lower temperature (below ~615°C at ~6 kbar; Figure 3a). The staurolite stability range has an upper temperature limit of 635–685°C at 5–10.5 kbar and a lower temperature limit of 600–610°C at 5–7 kbar (Figure 3a). Thus, the observed pre-peak and/or peak st–ky-bearing mineral assemblages and the post-peak cummingtonite-bearing assemblages are in agreement with a *P–T* path involving decompression.

The compositional isopleths involving Ti in biotite, An in plagioclase and $Mg^{\#}$ and X_{Ca} in garnet were contoured in the relevant assemblage fields (Figure 3b). The measured Ti(bi) of 0.092–0.116 yields a temperature range of 630–680°C. In the proposed pre-peak and/or peak assemblage fields, g + ky ±st + ru +bi + pl +q, the measured maximum $Mg^{\#}$(g) of 29.1 yields a peak temperature of ~670°C; additionally, the measured minimum An(pl) of 31.3 yields a peak pressure of ~10.5 kbar in the kyanite-bearing fields (Figure 3b). Therefore, the peak *P–T* condition is estimated to be ~10.5 kbar and ~675°C (B in Figure 3b), which is recorded by the maximum $Mg^{\#}$(g) and Ti(bi) as well as the minimum An(pl). A pre-peak *P–T* condition of ~9.5 kbar and ~620°C (A in Figure 3b) is approximately constrained by the minimum Ti(bi), in the staurolite-bearing fields. In contrast, in the cummingtonite-bearing assemblage field, g + st +cum + ilm +pl + bi +q (Figure 3b), the isopleths of X_{Ca} (6.2–7.2) and $Mg^{\#}$ = 25.3 in garnet rim yield a retrograde *P–T* condition of ~6.5 kbar and ~670°C (C in Figure 3b). Moreover, the chlorite present in the matrix and garnet cracks should form below ~610°C (D in Figure 3b).

5 | GEOCHRONOLOGY AND HAFNIUM ISOTOPE

5.1 | U–Pb age and Hf isotope of detrital zircon

The Cathodoluminescence (CL) images of representative detrital zircon with $^{206}Pb/^{238}U$ dates are shown in Figure S3a. The zircon grains are commonly prismatic, 50–150 μm in size and show intermediate luminescence with very narrow metamorphic overgrowths. The zircon grains are multi-source, as inferred from their morphologies, in that some have cores with clear oscillatory zoning whereas others possess almost homogeneous cores (Figure S3a). The 120 analysed detrital zircon grains yield $^{206}Pb/^{238}U$ dates from 445 ± 4 Ma to 2,237 ± 22 Ma (Figure 4a; Table S3). The frequency distribution shows a highlighted high frequency of 63 young dates (445–539 Ma), with the youngest age peak at ~ 460 Ma (Figure 4a), which is regarded as the maximum limit of the depositional age. The zircon grains with young ages have $\varepsilon_{Hf}(t)$ values between − 7.0 and 12.5, implying a contribution of juvenile materials from a depleted mantle source and re-melting of old crust (Figure 4b; Table S4).

5.2 | U–Pb age of metamorphic monazite

Back-scattered electron (BSE) images of representative monazites with $^{206}Pb/^{238}U$ dates are shown in Figure S3b. The monazites are commonly subhedral to oval in shape and ~ 100 μm in size. In BSE images, they appear homogeneous in dark grey with few inclusions. The chondrite-normalized REE pattern of the monazite (Figure 4c) shows

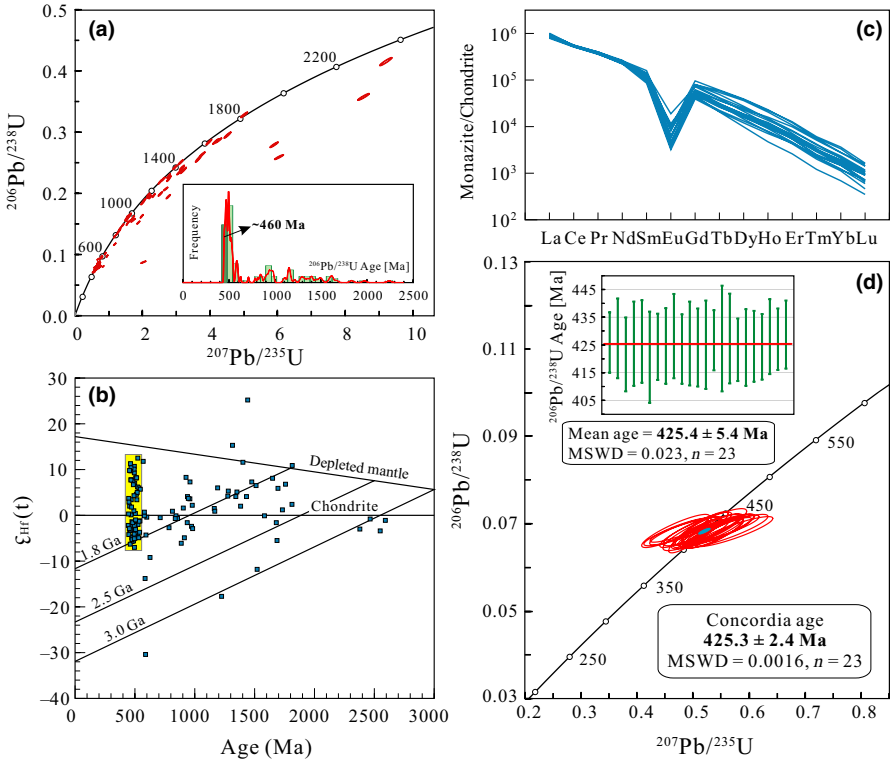

FIGURE 4 (a) U–Pb concordia diagram and age frequency distribution of detrital zircon. (b) Hf isotope data of the detrital zircon. (c) Chondrite-normalized REE patterns of metamorphic monazite. (d) Concordant and weighted mean age of metamorphic monazite [Colour figure can be viewed at wileyonlinelibrary.com]

right-sloped variations with reduced concentrations, significant negative Eu anomalies and $(Gd/Lu)_N$ of 37–131. The 23 analysed monazite grains yield $^{206}Pb/^{238}U$ dates from 420.6 ± 16.4 Ma to 428.9 ± 12.3 Ma (Table S5), with a concordia age of 425.4 ± 2.4 Ma and a weighted mean $^{206}Pb/^{238}U$ age of 425.4 ± 5.4 Ma (Figure 4d), which is interpreted to represent the metamorphic age of the metasedimentary rocks.

6 | DISCUSSION

6.1 | Formation and metamorphism of the sedimentary rocks

The detrital zircon in the metasedimentary rocks exhibits a dominant age frequency at 445–539 Ma, which overlaps with the timing of arc magmatism (429–515 Ma) in central Qilian (Yan, Xiao, Windley, Wang, & Li, 2010). In conjunction with the Hf isotope characteristics, the age distribution supports an arc setting for the sedimentary protolith, either a fore-arc (Xiao et al., 2009; Yan et al., 2010; Zuza et al., 2018) or a back-arc basin (Du, Zhu, Han, & Gu, 2004; Song et al., 2013). Some Mesoproterozoic and Neoproterozoic zircon grains were probably shed from the Precambrian basement (Figure 1b).

From the petrologic analyses and phase equilibria modelling, the estimated metamorphic *P–T* conditions yield a clockwise *P–T* path for the metasedimentary rocks beneath the Dingxi Basin, comprising a pre-peak compressional heating stage at 9.5–10.5 kbar (Stage I; A → B in Figure 3b), a subsequent post-peak isothermal decompression stage at ~ 670°C down to ~ 6.5 kbar (Stage II; B → C in Figure 3b) and a later cooling stage (Stage III; C → D in Figure 3b). During stage I, garnet and kyanite grew by consumption of hydrous minerals, such as chlorite and staurolite. During stage II, only minor cummingtonite formed by consuming garnet and kyanite, which implies that the influx of H_2O is not significant. The REE characteristics of the monazite involving depleted HREE with $(Gd/Lu)_N$ of 37–131 and negative Eu anomalies (Figure 4c) suggest that it was in equilibrium with voluminous garnet and was accompanied by plagioclase growth (Hermann & Rubatto, 2003; Rubatto, Hermann, & Buick, 2006). The mode isopleths of garnet and plagioclase (Figure 3a) indicate the monazite most likely formed during the decompression stage (stage II). Therefore, the monazite age (~425 Ma) should reflect the post-peak isothermal decompression stage.

6.2 | Tectonic constraints for the evolution of NQO

The constructed clockwise *P–T* path for the metasedimentary rocks corresponds to a burial–exhumation process. The pre-peak and peak *P–T* conditions exhibit an intermediate geotherm of ~ 21°C/km in the medium-pressure facies series, implying crustal thickening most likely related to the collision between the Qilian–Qaidam and the Alashan blocks. The correlation is also supported by the maximum depositional age of ~ 460 Ma and the metamorphic age of ~ 425 Ma reported in this study.

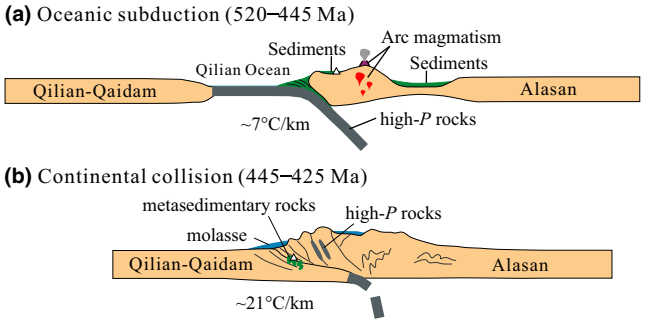

FIGURE 5 Sketch of the geologic scenario. The triangle indicates the position of the studied samples [Colour figure can be viewed at wileyonlinelibrary.com]

Based on the current data, the transitional scenario from oceanic subduction to continental collision in NQO can be elucidated as follows. The oceanic subduction was proposed to have initiated at ~520 Ma (Song et al., 2013), as inferred from the ~517 Ma boninite terrane (Xia, Song, & Niu, 2012) and >500 Ma arc magmatism (Wu et al., 2010), with a typical geotherm of ~7°C/km for this stage (Figure 5a). The transition from oceanic subduction to continental collision occurred at ~ 445 Ma (Song et al., 2013), as suggested by the latest arc volcanic rock at ~446 Ma (Wang, Zhang, Qian, & Zhou, 2005) and the 446–454 Ma blueschist (Liu et al., 2006). This study supports that the collision process proceeded and culminated between 445 and 425 Ma with a geotherm of ~21°C/km (Figure 5b), which is consistent with the development of the Lower Devonian molasse (Song et al., 2013). In conclusion, the sedimentary rocks beneath the Dingxi Basin experienced a complete cycle of deposition–burial–exhumation and thus record the corresponding evolution from subduction to collision.

ACKNOWLEDGEMENTS

Constructive suggestions and comments from the editor Klaus Mezger and two anonymous reviewers led to great improvements in the quality of this article. The study was financially supported by the National Natural Science Foundation of China (41672062, 41202047) and the Fundamental Research Funds of the Chinese Academy of Geological Sciences (JYYWF201819).

DATA AVAILABILITY STATEMENT

The data in this study are available for sharing.

ORCID

Bin Wang https://orcid.org/0000-0002-7635-6535

REFERENCES

Brown, M. (2001). From microscope to mountain belt: 150 years of petrology and its contribution to understanding geodynamics, particularly the tectonics of orogens. *Journal of Geodynamics*, *32*(1–2), 115–164. https://doi.org/10.1016/S0264-3707(01)00018-7

Chen, Y. X., Song, S. G., Niu, Y. L., & Wei, C. J. (2014). Melting of continental crust during subduction initiation: A case study from the Chaidanuo peraluminous granite in the North Qilian suture

zone. *Geochimica Et Cosmochimica Acta*, *132*, 311–336. https://doi.org/10.1016/j.gca.2014.02.011

Du, Y., Zhu, J., Han, X., & Gu, S. (2004). From the back-arc basin to foreland basin-Ordovician-Devonian sedimentary basin and tectonic evolution in the North Qilian orogenic belt. *Geological Bulletin of China*, *23*, 911–917.

Feng, Y. M., & He, S. P. (1996). *Geotectonics and orogeny of the Qilian Mountains*. Beijing: Geological Publish House.

Hermann, J., & Rubatto, D. (2003). Relating zircon and monazite domains to garnet growth zones: Age and duration of granulite facies metamorphism in the Val Malenco lower crust. *Journal of Metamorphic Geology*, *21*, 833–852. https://doi.org/10.1046/j.1525-1314.2003.00484.x

Lin, Y. H., Zhang, L. F., Ji, J. Q., & Song, S. G. (2010). $^{40}Ar/^{39}Ar$ age of Jiugequan lawsonite blueschists in northern Qilian Mountains and its petrologic significance. *Chinese Science Bulletin*, *55*, 2021–2027.

Liou, J. G., Wang, X., Coleman, R. G., Zhang, Z. M., & Maruyama, S. (1989). Blueschists in major suture zones of China. *Tectonics*, *8*, 609–619. https://doi.org/10.1029/TC008i003p00609

Liu, Y. J., Neubauer, F., Genser, J., Takasu, A., Ge, X. H., & Handler, R. (2006). $^{40}Ar/^{39}Ar$ ages of blueschist facies pelitic schists from Qingshuigou in the Northern QilianMountains, western China. *Island Arc*, *15*, 187–198. https://doi.org/10.1111/j.1440-1738.2006.00508.x

Rubatto, D., Hermann, J., & Buick, I. S. (2006). Temperature and bulk composition control on the growth of monazite and zircon during low-pressure anatexis (Mount Stafford, Central Australia). *Journal of Petrology*, *47*, 1973–1996. https://doi.org/10.1093/petrology/egl033

Shi, R. D., Yang, J. S., & Wu, C. L. (2004). First SHRIMP dating for the formation of the Late Sinian Yushigou Ophiolite North Qilian Mountains. *Acta Geologica Sinica*, *78*, 649–657. (in Chinese with English abstract)

Song, S. G. (1996). *Metamorphic geology of blueschists, eclogites and ophiolites in the North Qilian mountains*. 30th IGC Field Trip Guide T392. Beijing: Geological Publishing House, 40 pp.

Song, S. G., Niu, Y. L., Su, L., & Xia, X. H. (2013). Tectonics of the North Qilian orogen, NWChina. *Gondwana Research*, *23*, 1378–1401. https://doi.org/10.1016/j.gr.2012.02.004

Song, S. G., Zhang, L. F., Niu, Y. L., Song, B., Zhang, G. B., & Wang, Q. J. (2004). Zircon U-Pb SHRIMP ages of eclogites from the North Qilian Mountains, NW China and their tectonic implication. *Chinese Science Bulletin*, *49*, 848–852.

Song, S. G., Zhang, L. F., Niu, Y. L., Wei, C. J., Liou, J. G., & Shu, G. M. (2007). Eclogite and carpholite-bearing metapelite in the North Qilian suture zone, NW China: Implications for Paleozoic cold oceanic subduction and water transport into mantle. *Journal of Metamorphic Geology*, *25*, 547–563.

Spear, F. S., Kohn, M. J., Florence, F. P., & Menard, T. (1991). Model for garnet and plagioclase growth in pelitic schists: Implications for thermometry and P-T path determinations. *Journal of Metamorphic Geology*, *8*, 683–696.

Tseng, C. Y., Yang, H. J., Yang, H. Y., Liu, D. Y., Tsai, C. L., Wu, H. Q., & Zuo, G. C. (2007). The Dongcaohe ophiolite from the North Qilian Mountains: A fossil oceanic crust of the Paleo-Qilian ocean. *Chinese Science Bulletin*, *52*, 2390–2401. https://doi.org/10.1007/s11434-007-0300-3

Wang, C. Y., Zhang, Q. I., Qian, Q., & Zhou, M.-F. (2005). Geochemistry of the Early Paleozoic Baiyin volcanic rocks (NW China): Implications for the tectonic evolution of the North Qilian Orogenic Belt. *Journal of Geology*, *113*, 83–94. https://doi.org/10.1086/425970

Wei, C. J., & Song, S. G. (2008). Chloritoid–glaucophane schist in the north Qilian orogen, NW China: Phase equilibria and P-T path from garnet zonation. *Journal of Metamorphic Geology*, *26*(3), 301–316. https://doi.org/10.1111/j.1525-1314.2007.00753.x

Wei, C. J., Yang, Y., Su, X. L., & Song, S. G. (2009). Metamorphic evolution of low-T eclogite from the North Qilian orogen, NW China: Evidence from petrology and calculated phase equilibria in the system NCKFMASHO. *Journal of Metamorphic Geology*, *27*, 55–70.

Wu, B. L., Deng, C. L., Kong, Y. F., & Liu, S. Z. (2018). Magnetostratigraphy of the fluvio-lacustrine sequence on the Guangongtan section in Longzhong Basin, NW China. *Chinese Journal of Geophysics*, *61*, 1390–1399. (in Chinese with English abstract).

Wu, C. L., Xu, X. Y., Gao, Q. M., Li, X. M., Lei, M., Gao, Y. H., … Wooden, J. L. (2010). Early Palaezoie granitoid magmatism and tectonic evolution in North Qilian, NW China. *Acta Petrologica Sinica*, *26*, 1027–1044. (in Chinese with English abstract)

Wu, H. Q., Feng, Y. M., Huo, Y. G., & Zuo, G. C. (1990). Discovery of lawsonite glaucophane schist and the signification in Sunan, Gansu, China. *Giological Review*, *36*, 277–280. (in Chinese with English Abstract).

Wu, H. Q., Feng, Y. M., & Song, S. G. (1993). Metamorphism and deformation of blueschist belts and their tectonic implications, North Qilian Mountains, China. *Journal of Metamorphic Geology*, *11*, 523–536. https://doi.org/10.1111/j.1525-1314.1993.tb00169.x

Xia, X. H., & Song, S. G. (2010). Forming age and tectono-petrogenises of the Jiugequan ophiolite in the North Qilian Mountain, NWChina. *Chinese Science Bulletin*, *55*, 1899–1907. https://doi.org/10.1007/s11434-010-3207-3

Xia, X. H., Song, S. G., & Niu, Y. L. (2012). Tholeiite-Boninite terrane in the North Qilian suture zone: Implications for subduction initiation and back-arc basin development. *Chemical Geology*, *328*, 259–277. https://doi.org/10.1016/j.chemgeo.2011.12.001

Xiang, Z. Q., Lu, S. N., Li, H. K., Li, H. M., Song, B., & Zheng, J. K. (2007). SHRIMP U-Pb zir con age of gabbro in Aoyougou in the western segment of the North Qilian Mountains, China and its geological implications. *Geological Bulletin of China*, *26*, 1686–1691.

Xiao, W., Windley, B. F., Yong, Y., Yan, Z., Yuan, C., Liu, C., & Li, J. (2009). Early Paleozoic to Devonian multiple-accretionary model for the Qilian Shan, NW China. *Journal of Asian Earth Sciences*, *35*, 323–333. https://doi.org/10.1016/j.jseaes.2008.10.001

Yan, Z., Xiao, W. J., Windley, B. F., Wang, Z. Q., & Li, J. L. (2010). Silurian clastic sediments in the North Qilian Shan, NW China: Chemical and isotopic constraints on their forearc provenance with implications for the Paleozoic evolution of the Tibetan Plateau. *Sedimentary Geology*, *231*, 98–114. https://doi.org/10.1016/j.sedgeo.2010.09.001

Yang, J. H., Du, Y. S., Cawood, P. A., & Xu, Y. J. (2012). From subduction to collision in the Northern Tibetan Plateau: Evidence from the Early Silurian clastic rocks, Northwestern China. *Journal of Geology*, *120*, 50–68. https://doi.org/10.1086/662717

Yang, H., Zhang, H., Luo, B., Zhang, J., Xiong, Z., & Guo, L. (2015). Early paleozoic intrusive rocks from the eastern qilian orogen, NE Tibetan plateau: Petrogenesis and tectonic significance. *Lithos*, *224–225*, 13–31.

Yang, H., Zhang, H., Luo, B., Zhang, J., Xiong, Z., & Guo, L. (2014). Consensus guidelines of ECCO/ESPGHAN on the medical management of pediatric Crohn's disease. *Journal of Crohn's & colitis*, *8*(10), 1179–1207. https://doi.org/10.1016/j.crohns.2014.04.005.

Zhang, Q., Chen, Y. & Zhou, D. J. (1998). Geochemical characteristics and genesis of Dachadaban ophiolite in North Qilian area. *Science in China Series D-Earth Science*, *41*(3), 277–281. https://doi.org/10.1007/BF02973116

Zhang, J. X., Meng, F. C., & Wan, Y. S. (2007). A cold Early Palaeozoic subduction zone in the North Qilian Mountains, NW China: Petrological and U-Pb geochronological constraints. *Journal of Metamorphic Geology*, *25*, 285–304. https://doi.org/10.1111/j.1525-1314.2006.00689.x

Zhang, J. X., Xu, Z. Q., Chen, W., & Xu, H. F. (1997). A tentative discussion on the ages of the subduction-accretionary complex/volcanic arcs in the middle sector of North Qilian Mountain. *Acta Petrologica Et Mineralogica*, *16*, 112–119. (in Chinese with English abstract).

Zhang, Q., Sun, X., Zhou, D., Qian, Q., Chen, Y., Wang, Y., … Han, S. (1997). The characteristics of North Qilian ophiolites, forming settings and their tectonic significance. *Advance in Earth Sciences*, *12*, 366–393. (in Chinese with English abstract).

Zuza, A. V., Wu, C., Reith, R. C., Yin, A., Li, J., Zhang, J., … Liu, W. (2018). Tectonic evolution of the Qilian Shan: An early Paleozoic orogen reactivated in the Cenozoic. *GSA Bulletin*, *130*, 881–925. https://doi.org/10.1130/B31721.1

SUPPORTING INFORMATION

Additional supporting information may be found online in the Supporting Information section.

Figure S1. Photographs of the drill core and representative mineral microtextures.

Figure S2. Bulk-rock rare earth elements (REE) patterns.

Figure S3. Cathodoluminescence (CL) images of representative detrital zircon and back-scattered electron (BSE) images of representative metamorphic monazite.

Table S1. Compositions of selected garnet, plagioclase, biotite, staurolite and cummingtonite.

Table S2. Measured bulk-rock compositions.

Table S3. U–Pb isotopic data for detrital zircon.

Table S4. Hf isotopic data for detrital zircon.

Table S5. U–Pb isotopic data for metamorphic monazite.

Appendix S1. Analytical and calculation methods.

How to cite this article: Wang B, Wang W-(RZ), Tian Z, Wei C, Zhao Y. Formation and metamorphism of sedimentary rocks beneath the Dingxi Basin: Record of the evolution from subduction to collision in the North Qilian Orogen. *Terra Nova*. 2020;32:198–204. https://doi.org/10.1111/ter.12447